DEPLOYABLE DIRECT RADIATING ARRAY ANTENNAS FOR CUBESAT APPLICATIONS

Alan Thompson(1), Martin S. Thompson(2)

(1)Eureco Technologies Ltd, 2 Puckpool Hill, Ryde, Isle of Wight, PO33 1PJ, UK, Email: a.thompson@eureco.com
(2)Eureco Technologies Ltd, Email: m.thompson@eureco.com

Abstract – The eureco® EM-bridge™ is an enabling technology for use in direct radiating array antennas. The results of a co-funded Innovate UK project have validated the technology readiness level of different microstrip versions of the eureco® EM-bridge™ to TRL4. A current ESA Innovation Triangle Initiative (ESA-ITI) activity will validate the technology to TRL5 Excellent mechanical properties and outstanding RF performance also provide unique benefits for conveying RF energy in deployable structures such as booms and robotic arms.

I. INTRODUCTION

The eureco® EM-bridge™ was conceived to address issues in beam-forming networks (BFNs) of very large aperture direct radiating array (DRA) antennas. At low frequencies, the BFN typically uses coaxial cable technology but launch vehicle, stowage and deployment requirements impose design constraints that exacerbate BFN losses. Other issues include excessive resistive torque and passive intermodulation (PIM). Novel planar transmission line coupling elements were invented to circumvent these issues.

At the 36th ESA Antenna Workshop on Antennas and RF Systems for Space Science, the authors of this paper introduced the concept of planar transmission line coupling elements for use in deployable array DRA antennas and in other structures, such as feeds for reflector antennas, booms and robotic arms that may be deployed from a satellite platform. [1].

In this paper, we

- review the issues in deployable DRA antennas,
- illustrate an invention that avoids these issues,
- present some of the results obtained from computer simulation models,
- present S-parameter measurements of breadboard items,
- outline our business model, and
- discuss future activities to enhance the technology readiness level of the invention.

II. DEPLOYABLE DRA ANTENNA ISSUES

A radio frequency (RF) harness, comprising a large number of long coaxial cables, is typically used as part of a BFN to make signal path connections between transmit/receive modules (TRMs), located in a central region of a satellite, and subarrays of radiating elements distributed across the large aperture of a low frequency antenna. RF harness issues are associated with the following parameters:

- Attenuation
- Phase stability
- Passive intermodulation
- Resistive torque
- Mass

For a given form of construction and materials content in a coaxial cable, the attenuation due to conductor losses is inversely proportional to the diameter of its dielectric and directly proportional to the square root of frequency. Dielectric loss is independent of the cable diameter and is directly proportional to frequency.

The phase stability of a coaxial cable is critically dependent on its form of construction, the materials content and the extent to which it is bent and twisted.

Non-linearities at the metal-to-metal contacts in the coaxial connectors and in the braid along the lengths of the coaxial cable, feeding the subarrays in an antenna, can cause severe PIM issues [2, 3]. Special connectors and assembly procedures are required to meet demanding PIM requirements. PIM interference can have a serious impact on the performance of high-power multi-frequency telecommunication systems, especially when the antenna is shared simultaneously by the transmitter and the receiver. The resistive torque of a RF cable harness becomes an issue when the cable diameter and the number of cables are increased. Although the resistive torque of the cable can be reduced by means of a cable drum at each inter-panel junction, neither the cables nor the cable drums contribute to the stiffness of the antenna and such an arrangement is cumbersome. Furthermore, at low temperature the resistive torque of a RF cable harness increases, thus exacerbating the problem and escalating the risk of a deployment failure.

III. THE EURECO® EM-BRIDGE™

The coupling elements, described in [1], are now being licensed and marketed as the eureco® EM-bridge™, which is an enabling technology offering the dual function of:

(a) assisting, or enabling, the deployment of antenna panels by means of stored mechanical strain energy, and

(b) providing an extremely efficient transfer of electromagnetic energy across each inter-panel gap, without recourse to metal-to-metal contact.

In a coaxial connector-pair coupling assembly, the RF performance is dependent on achieving and maintaining a low resistance at the conductor interfaces. Abrasion and corrosion at these interfaces are sources of failure in RF subsystems. In contrast, the RF performance of the eureco® EM-bridge™ does not rely on a metal-to-metal contact and therefore the performance in the frequency range of interest is superior to that of a coaxial cable assembly. The absence of a metal-to-metal contact ensures that PIM issues are minimized or eliminated.

The eureco® EM-bridge provides a convenient interface with microstrip and stripline RF transmission lines, whose format is ideally suited for realising low-mass, high-stiffness panels for accommodating the BFN and the subarrays of radiating elements.

Fig. 1 illustrates the eureco® EM-bridge in its microstrip form. For reasons of clarity, neither the ground plane nor the hinge is shown. The flexible trace is fixed to the lower/right hand panel but it is free to move on the upper/left hand panel. In Fig. 1a, the stored mechanical strain energy and the torque available for deployment are both at their maximum.

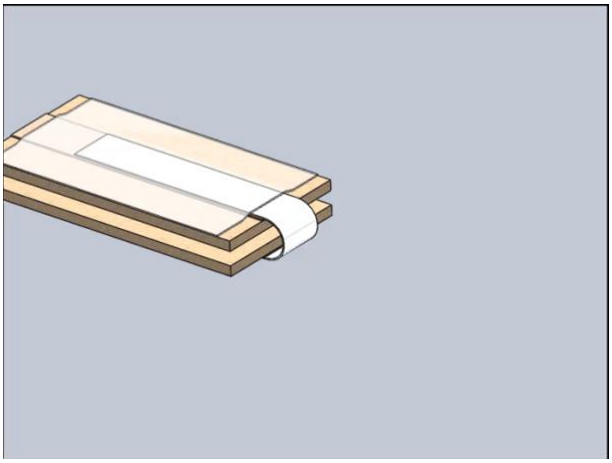

Figure 1a: The eureco® EM-bridge™ in a fully folded (stowed) state, where the stored mechanical strain energy and the available torque are at their maximum.

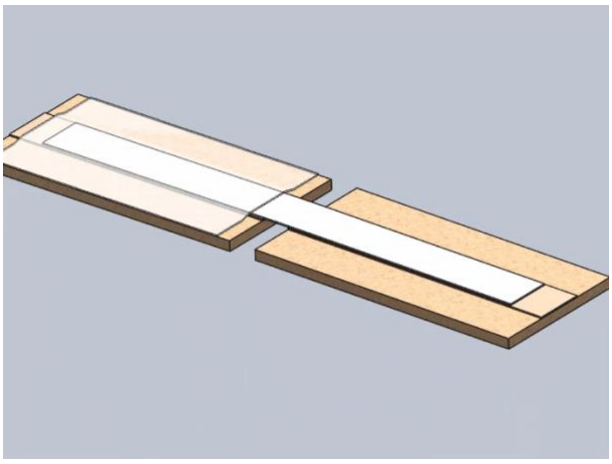

Figure 1b: The eureco® EM-bridge™ in a fully deployed state.

The flexible trace is separated from each of the respective microstrip traces by a dielectric medium, thus forming two series-branches (also known as series stubs) of low-impedance, parallel-plate transmission line. The flexible ground plane can either be common to both of the microstrip transmission lines, or can be of a similar form to the flexible trace. Each series-branch is nominally a quarter-wavelength long at the operating frequency and is terminated in an open circuit, which is transformed to a short circuit at each bridge abutment by means of the impedance inverter property of the quarter-wavelength line. Each short circuit (or very low impedance) provides RF continuity for the respective flexible traces (and flexible ground planes) to facilitate a bridging microstrip transmission line connection between the adjacent sections of the microstrip transmission line. A relatively large bandwidth is possible if a high ratio is maintained for the respective characteristic impedances of the main microstrip transmission line and the series branches.

The mechanical and electrical behaviour of the eureco® EM-bridge™ has been modelled and simulated to give a better understanding of the physics involved. In-house additive manufacture (AM) was used to 3D print breadboard versions of the eureco® EM-bridge™ and a network analyser was used to assess their performance.

V. MECHANICAL MODELLING AND SIMULATION

COMSOL Multiphysics and the Structural Mechanics Module were used to develop a basic 2D model to simulate the mechanical behaviour of a thin (0.25mm) flexible polyethylene terephthalate (PET) strip, a part of which is constrained in one panel and the other part is free to slide inside a polytetrafluoroethylene (PTFE) guide that is contained within a rotatable panel. A Young's modulus value of 3e9Pa and a Poisson's ratio of

0.38 were used for the PET material properties. The static frictional coefficient for the PTFE guide interface was set to a low value of 0.01. The results of the simulation were normalised to a strip width of 1m.

The rotatable panel was displaced in angular steps of 1º from its fully deployed position (0º) through to its fully folded (stowed) position (-180º), where the strip took up the shape shown in Fig. 2. The computed shape is similar to the actual shape observed when a strip of PET material is folded into this position. Fig. 3 shows that the computed von Mises stress within the strip has a maximum value of 2.23e6 N/m.

Torque has been computed as the product of the tangent of the force vector and the offset between the centre of mass of the rigid domain and the centre of rotation of the rigid domain in cylindrical coordinates. Fig. 4 shows the torque plotted against angular displacement. The total elastic strain energy is plotted against angular displacement in Fig. 5.

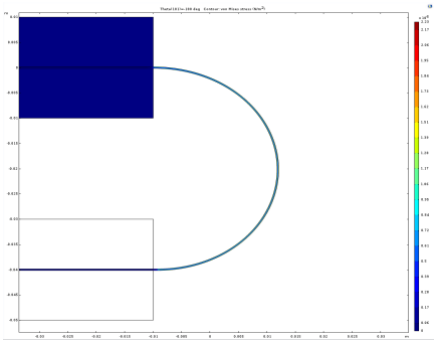

Figure 2: The computed shape of the PET strip in a fully folded state (-180º rotation).

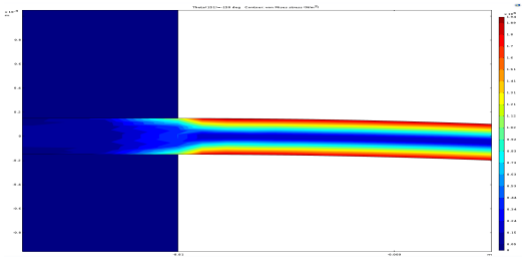

Figure 3: The computed von Mises stress within the PET strip for a fully folded state (-180º rotation).

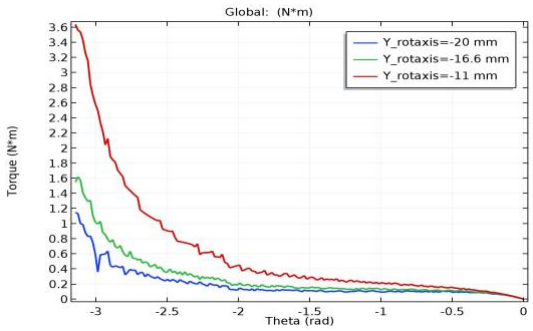

Figure 4: The computed torque as a function of angular displacement with rotation radii as parameter.

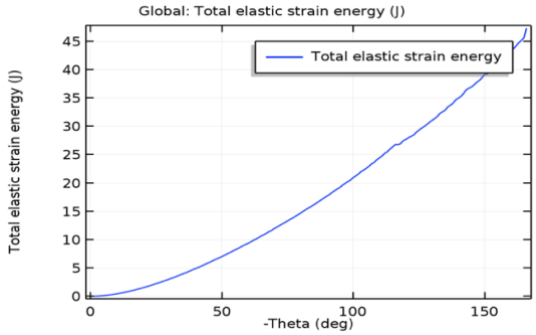

Figure 5: The computed total elastic strain energy vs angular displacement for a rotation radius of 20mm.

B. RF Modelling and Simulation

VIII. CUBESAT APPLICATIONS OF GNSS

Since the introduction of the Global Positioning System (GPS) in 1978, several alternative systems have evolved and the generic term Global Navigation Satellite System (GNSS) is now used for such systems.

Space-borne GNSS receivers are no longer limited to spacecraft positioning. Signals from GNSS have been used with varying success for remote sensing: radio occultation (GNSS-RO), reflectometry (GNSS-R), and other applications such as interference detection.

GNSS-RO has become a relatively well accepted operational technique of sensing GNSS signals, providing useful data into terrestrial and space weather models.

Compared to GNSS-RO, GNSS-R is in the development phase as far as satellite-based remote sensing is concerned, although the proposed G-TERN mission concept [RD11] potentially offers a significant advance in GNSS-R. By enabling constellations of satellites, these architectures have the potential to combine the temporal resolution of Geostationary Orbit (GEO) missions with the spatial resolution of Low Earth

Orbit (LEO) missions, thus changing the traditional trade-off in Earth Observation mission design.

In future GNSS-R missions, the available antenna area could be increased to yield an improved signal-to-noise ratio (S/N) by deploying antenna panels from a CubeSat. Fixed solar panels could be revealed when the side arrays are deployed and additional solar panels could be accommodated on the rear sides of the deployed antenna panels, thus augmenting the available energy for on-board processing.

The number of parts of the deployable antenna arrays can be minimised and the transfer of RF energy can be simplified by using a continuous ground plane of beryllium copper sheet, which can be folded around the corners of the CubeSat to store mechanical strain energy in the stowed configuration (Fig. 6).

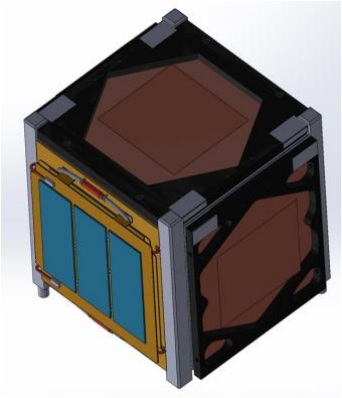

Figure 6: A rendered image of a deployable DRA antenna in its stowed state.

When in orbit, the CubeSat is ejected from the Pod and the stored mechanical stored energy is used to deploy the antenna arrays (Fig.7).

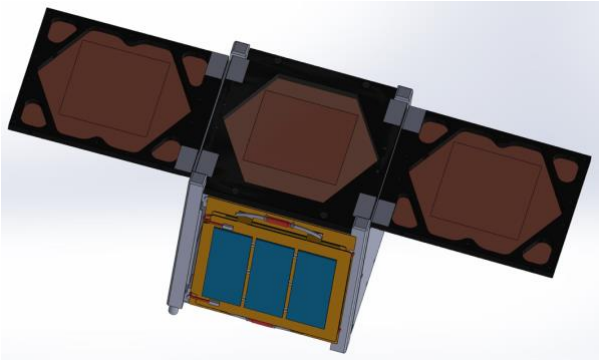

Figure 7: A rendered image of a deployable S-band DRA antenna in its deployed state.

A simplified equivalent circuit of a eureco® EM-bridge™ comprising a continuous ground plane and a series stub in the trace of a microstrip transmission line is shown in Figure 8.

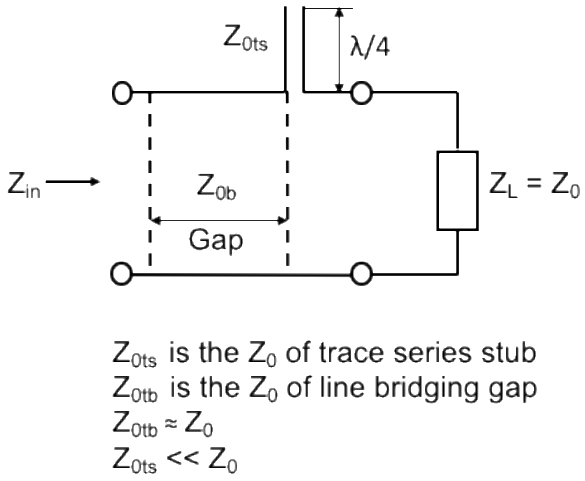

Figure 8 A simplified equivalent circuit of an EM-bridge comprising a continuous ground plane and series stub in the trace.

The bandwidth of the EM-bridge is mainly determined by the ratio of the characteristic impedances of the microstrip and parallel-plate transmission lines. MATLAB and the RF Toolbox were used to analyse the simplified equivalent circuit for the whole of the GNSS frequency band. Plots of |S11|dB and |S21|dB vs frequency for the overall response of the lossless GNSS eureco® EM-bridge™ are shown in Fig. 9 and Fig. 10 respectively for an impedance ratio of approximately 10:1.

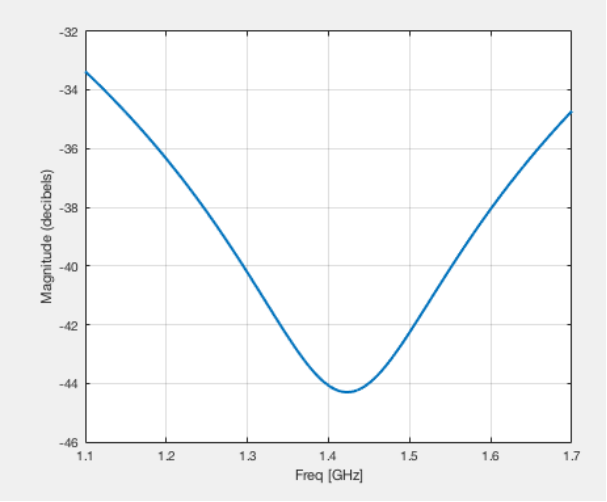

Figure 9 Plot of |S11|dB vs frequency for the overall response of the lossless GNSS eureco® EM-bridge™ when the ratio of characteristic impedances of the microstrip and parallel-plate transmission lines is approximately 10:1

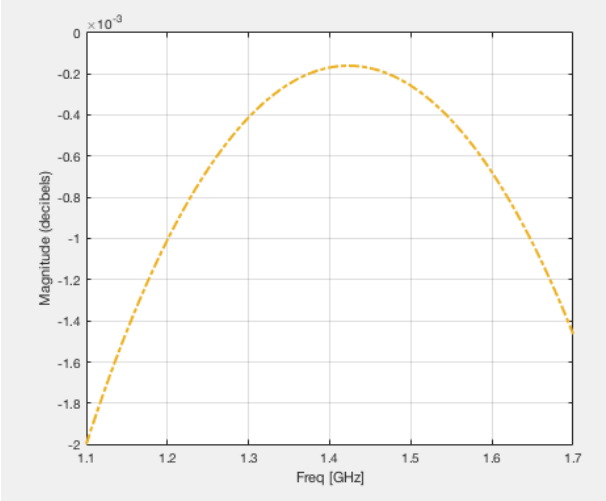

Figure 10 Plot of |S21|dB vs frequency for the overall response of the lossless GNSS eureco® EM-bridge™ when the ratio of characteristic impedances of the microstrip and parallel-plate transmission lines is approximately 10:1.

Fig. 11 and Fig. 12 show plots of S11|dB and |S21|dB vs frequency for the lossy case, i.e. accounting for conductor and dielectric losses.

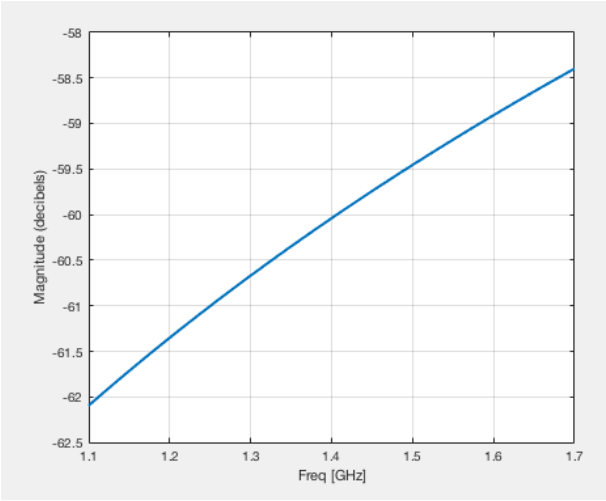

Figure 11 Plot of |S11|dB vs frequency for the overall response of the lossy GNSS eureco® EM-bridge™ when the ratio of characteristic impedances of the microstrip and parallel-plate transmission lines is approximately 10:1.

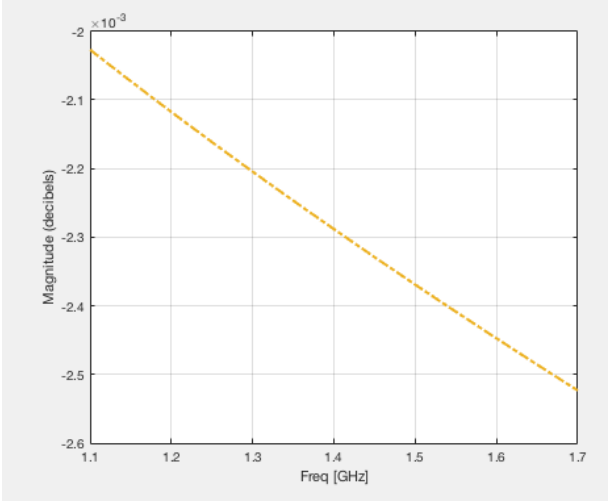

Figure 12 Plot of |S21|dB vs frequency for the overall response of the lossy GNSS EM-bridge when the ratio of characteristic impedances of the microstrip and parallel-plate transmission lines is approximately 10:1.

VIII. DEPLOYABLE S-BAND ANTENNAS FOR CUBESAT MISSIONS

High resolution imaging demands a wider bandwidth and a higher operational frequency for data transmission. S-band is an attractive compromise in terms of path loss, all-weather operation and efficient RF power generation. High-performance antennas for CubeSats are challenging due to their small physical dimensions. However, deployable DRA antennas are compatible with the geometric and modular form of the CubeSat.

CubeSats, equipped with S-band antennas, are an attractive proposition for use in Meteorological Data Acquisition [*] and other environmental monitoring applications.

The geometry of a deployable aperture-couple S-band patch antenna, developed within the ESA-ITI activity, is shown in Fig. 13.

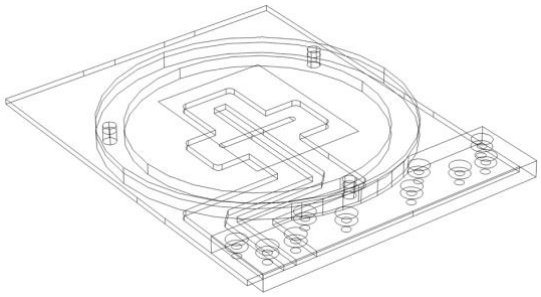

Figure 13 Geometry of a deployable aperture-couple S-band patch antenna, developed within the ESA-ITI activity.

COMSOL Multiphysics and the RF Module were used to model the aperture-couple S-band patch antenna. Plots of S11|dB vs frequency for the simulation and RF measurement are shown in Fig. 14 and Fig. 15 respectively.

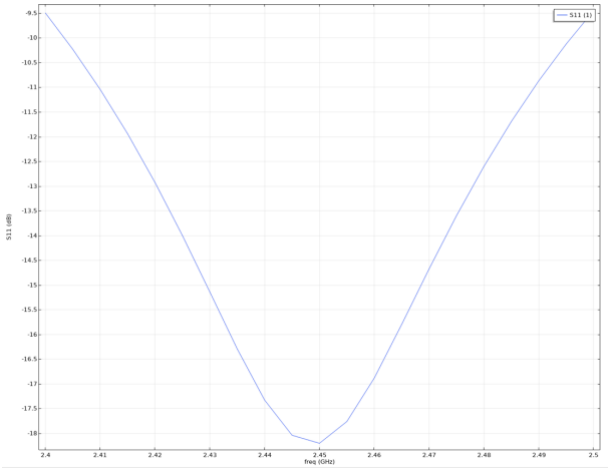

Figure 14 Simulated result of |S11|dB vs frequency for the deployable aperture-couple S-band patch antenna.

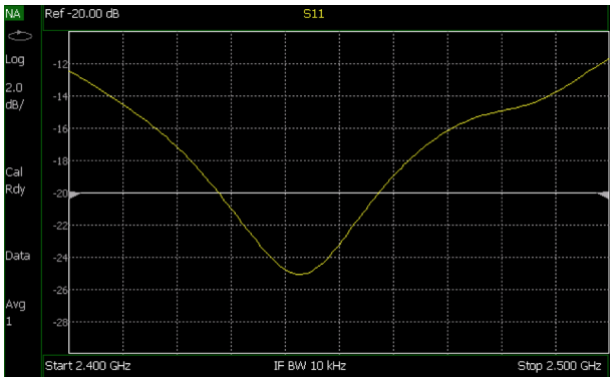

Figure 15 RF measurement of |S11|dB vs frequency for the deployable aperture-couple S-band patch antenna.

Simulated 2D and 3D radiation patterns of the deployable aperture-couple S-band patch antenna are shown in Fig. 16 and Fig. 17 respectively.

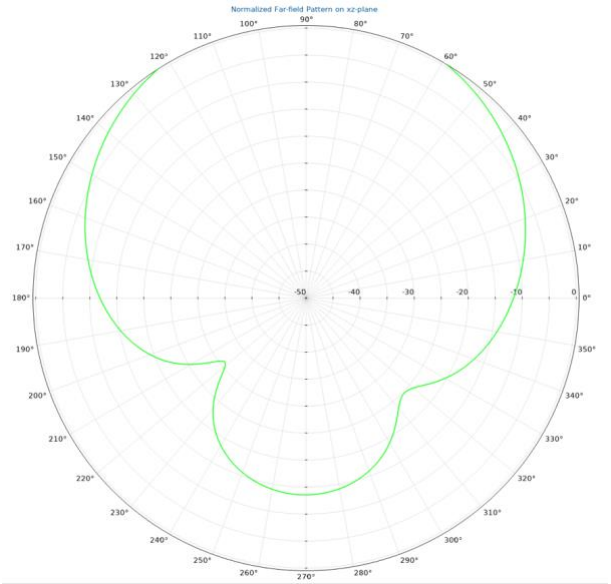

Figure 16 Normalised far-field pattern on the xz-plane for the deployable aperture-couple S-band patch antenna.

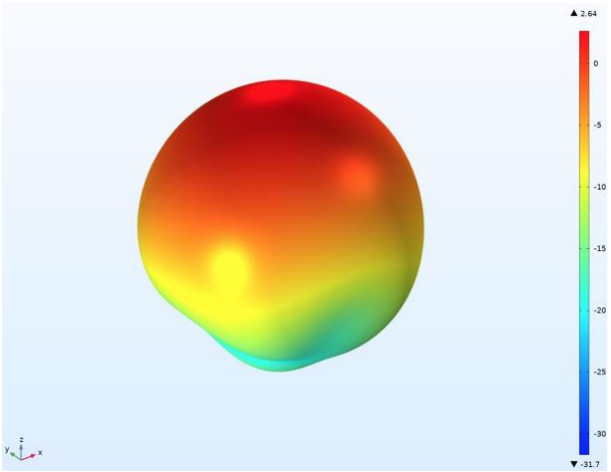

Figure 17 3D far-field pattern for the deployable aperture-couple S-band patch antenna.

In order to reduce the S-Band down-link transmitter power requirement, the above-mentioned (linearly polarised) deployable aperture-couple S-band patch antenna has been adapted for use in a deployable cruciform array, shown in Fig. 18, to produce circular polarisation by means of a sequential 90 degree phase rotation.

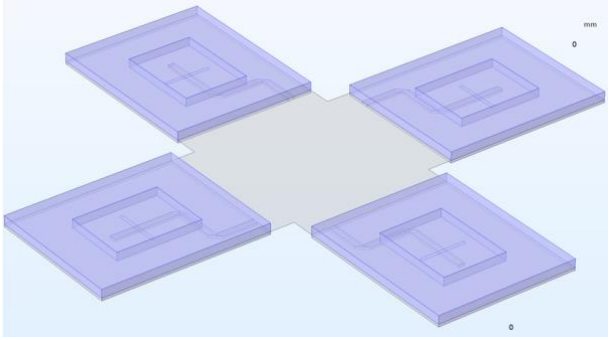

Figure 18 Geometry of a deployable aperture-couple S-band four element cruciform antenna to produce circular rotation.

The geometry of a phase rotation BFN, comprising a rat-race coupler feeding two branch-arm couplers, for the the deployable aperture-coupled S-band four element cruciform antenna, is shown in Fig. 19.

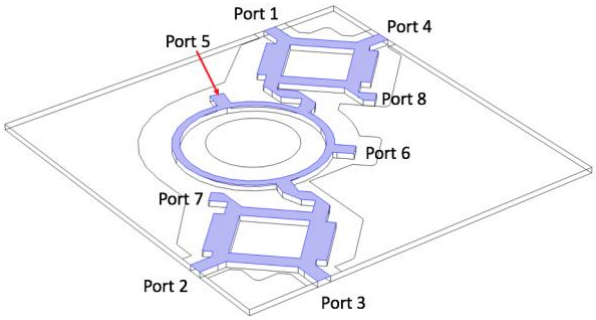

Figure 19 Geometry of the phase rotation BFN for the the deployable aperture-couple S-band four element cruciform antenna.

The computed 3D radiation pattern for the deployable aperture-couple S-band four element cruciform antenna is shown in Fig. 20.

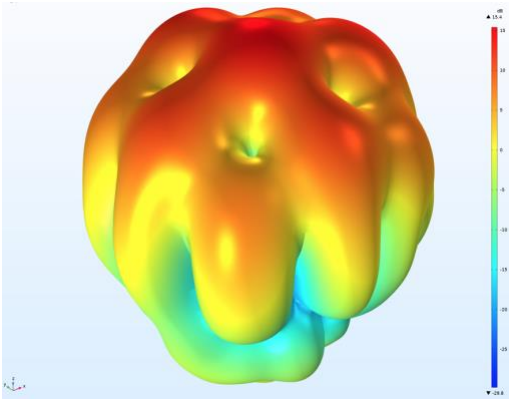

Figure 20 3D radiation pattern for the deployable aperture-couple S-band four element cruciform antenna.

Each of the four deployable antenna panels is interconnected to the central BFN by means of a eureco® EM-bridge™, whose geometry is shown in Fig. 21 Computed plots of S-parameters |S11| and |S21| for the eureco® EM-bridge™ are shown in Fig. 22 and Fig. 23 respectively.

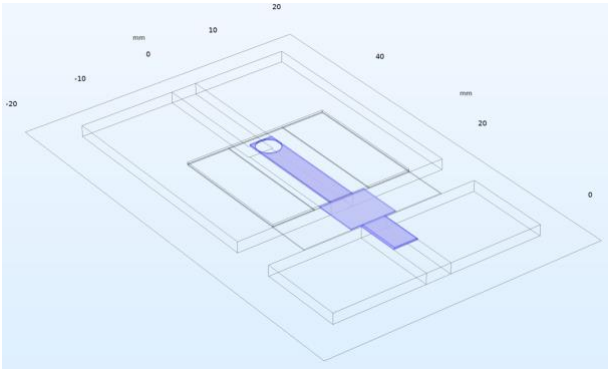

Figure 21 Geometry of the S-band eureco® EM-bridge™.

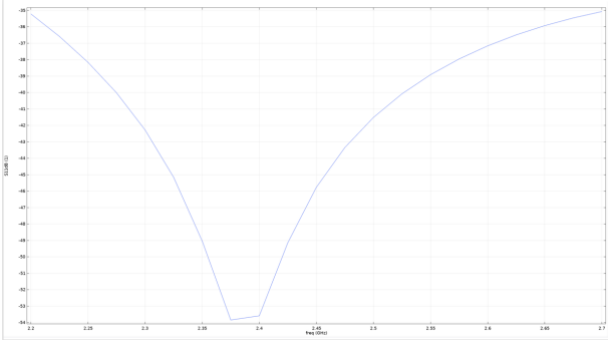

Figure 22 Plot of |S11| vs. frequency for *the S-band eureco® EM-bridge™.*

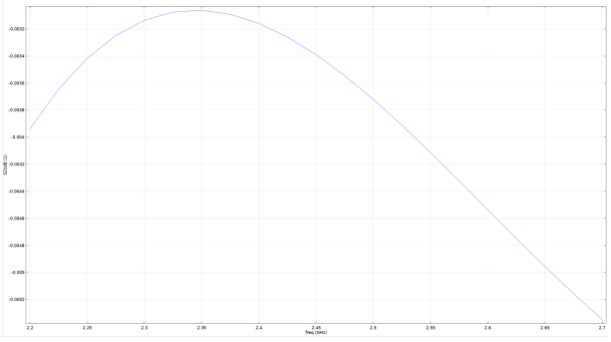

Figure 23 Plot of |S21| vs. frequency for *the S-band eureco® EM-bridge™.*

X. BUSINESS MODEL

In March 2017, the UK IPO granted a patent [10] for our invention. Encouraged by the excellent mechanical properties and the outstanding RF performance of the eureco® EM-bridge™, patent filings have been made at the European Patent Office (EPO), and at the respective patent offices in Australia, Canada, Hong Kong, India, Japan, Singapore, South Africa and the United States.

Working with strategic licensing partners and providing 3D-printed breadboards for evaluation are important aspect of our business model.

XI. FUTURE ACTIVITIES

Opportunities to increase the technology readiness level of the eureco® EM-bridge™ technology to beyond TRL5 for an in-orbit demonstrator mission space missions are being discussed with potential partners.

XII. CONCLUSION

Different microstrip versions of the eureco® EM-bridge™ have been validated to TRL4. The excellent mechanical properties and the outstanding RF performance of the eureco® EM-bridge™ provide a unique enabling technology for deployable DRA antennas and other structures, such as feeds for reflector antennas, booms and robotic arms that may be deployed from a satellite platform. Benefits include: higher antenna efficiency, improved stability of amplitude and phase, low PIM, low deployment torque and lower overall system mass. Lower BFN losses will allow a cost-effective centralisation of TRMs to benefit future SAR and telecommunication space missions. CubeSat applications are being identified.

XIII. ACKNOWLEDGEMENTS

The results presented in this paper are from activities performed in a completed co-funded Innovate UK project and from a current ESA Innovation Triangle Initiative.

XIV. REFERENCES

1. Thompson, A. & Thompson, M.S., (2015). Novel planar transmission line coupling elements for use in deployable antenna systems. *Proceedings of the 36th ESA Antenna Workshop on Antennas and RF Systems for Space Science.*

2. Bayrak, M., Eng, M. & Benson, F.A., (1975). Intermodulation Products from Nonlinearities in Transmission Lines and Connectors at Microwave Frequencies, *Proc. IEEE*, 122 (4).

3. Arazm, F. & Benson, F.A., (1980). Nonlinearites in Metal Contacts at Microwave Frequencies, *IEEE Transactions on Electromagnetic Compatibility*, EMC-22 (3).

4. Montesano, A., et al. (2012) Microstrip Array Technologies for Space. *Space Antenna Handbook*, Wiley Publication.

5. Saameno Perez, P. & Ludwig, M., (2008). Advanced digital beamforming architecture for synthetic aperture radar. *Proceedings of the 30th ESA Antenna Workshop on Antennas for Earth Observation, Science, Telecommunication and Navigational Space Missions.* 427-430

6. Additive Manufacturing for RF/Microwave Hardware (2016), ESA/ESTEC, Noordwijk, The Netherlands. https://indico.esa.int/event/154/

7. Thompson, A. et al, (2008). A Stepped-Aperture Antenna Concept for Low Frequency SAR Missions, *Proceedings of the 30th ESA Antenna Workshop on Antennas for Earth Observation, Science, Telecommunication and Navigation Space Missions*. 415-418.

8. Thompson, A. & Thompson, M.S., (2011). Deployable Panel Structure for an Array Antenna, US Patent No. 8,035,573B2.

9. Thompson, A. & Thompson, M.S., (2012). Deployable Panel Structure, UK Patent No. GB2455311B.

10. Thompson, A. & Thompson, M.S., (2017). Deployable radio frequency transmission line, Patent Grant GB2537885, *Intellectual Property Office Patents Journal*.

11. Cardellach, E et al., (2018) GNSS Transpolar Earth Reflectometry exploriNg System (G-TERN): Mission Concept, IEEE-Acess, 28 March 2018.

12. F. Ferreira, J. M., et al. (2017) Circularly Polarized Aperture-Coupled Microstrip Antenna for Nano-Satellites," in XXXV Simp´osio Brasileiro de Telecomunicacoes Processamento de Sinais S˜ao Pedro, Brazil, Sep. 2017, pp. 57–61.